

1 **On the selection of the anode material for the electrochemical**  
2 **removal of methylparaben from different aqueous media**

3 Juliana R. Steter, Enric Brillas<sup>#</sup>, Ignasi Sirés<sup>\*,#</sup>

4 *Laboratori d'Electroquímica dels Materials i del Medi Ambient, Departament de Química Física,*  
5 *Facultat de Química, Universitat de Barcelona, Martí i Franquès 1-11, 08028 Barcelona, Spain*

6 *Paper submitted to be published in **Electrochimica Acta***

7 \* Corresponding author: Tel.: +34 934039240; fax: +34 934021231.

8 E-mail address: i.sires@ub.edu (I. Sirés)

9 <sup>#</sup>Active ISE member

10

## 11 **Abstract**

12 Parabens are widely used industrial preservatives, routinely found in wastewater along with major  
13 inorganic ions like sulfate and chloride. This work investigates the oxidation ability of three  
14 electrochemical processes in tank reactors equipped with an air-diffusion cathode to electrogenerate  
15 H<sub>2</sub>O<sub>2</sub> on site, namely electro-oxidation (EO-H<sub>2</sub>O<sub>2</sub>), electro-Fenton (EF) and UVA photoelectro-  
16 Fenton (PEF), to degrade aqueous solutions of methylparaben (MeP) at pH 3.0. Their performance  
17 using boron-doped diamond (BDD), Pt or two kinds of dimensionally stable anodes (DSA<sup>®</sup>) has  
18 been compared from the analysis of mineralization profiles and decay kinetics in the presence of  
19 sulfate and/or chloride ions. The use of BDD ensured the overall mineralization in all three  
20 processes according to the sequence: PEF > EF > EO-H<sub>2</sub>O<sub>2</sub>, thanks to the contribution of  
21 BDD(•OH), •OH and UVA light. Pt and DSA<sup>®</sup> became an interesting alternative in PEF, with  
22 slower organic matter removal but similar final mineralization percentages, being much less  
23 powerful than BDD in EO-H<sub>2</sub>O<sub>2</sub>. The presence of Cl<sup>-</sup> was beneficial in the latter process, due to the  
24 formation of active chlorine as an additional oxidant that caused a much faster decay of MeP.  
25 Conversely, it became significantly detrimental in EF due to the partial destruction of H<sub>2</sub>O<sub>2</sub> and  
26 •OH in the bulk by active chlorine and Cl<sup>-</sup>, respectively. The oxidation power of PEF was so high  
27 that similar fast, complex decay kinetics was found in all media regardless of the anode, although  
28 the mineralization was decelerated owing to the accumulation of chlorinated by-products. GC-MS  
29 and HPLC analysis allowed the identification of up to seven aromatic MeP derivatives in sulfate +  
30 chloride mixtures, including three non-chlorinated compounds also found in pure sulfate medium.  
31 These molecules were gradually transformed into oxalic acid, along with four chlorinated aliphatic  
32 carboxylic acids in Cl<sup>-</sup>-containing media.

33 *Keywords:* BDD; DSA<sup>®</sup>; Methylparaben; Pt; Wastewater treatment

## 34 **1. Introduction**

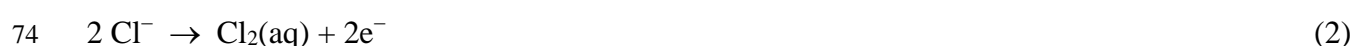
35        Nowadays, it is quite well established that the endocrine-disrupting chemicals cause adverse  
36 effects on the endocrine system of living beings, since they disrupt the physiological function of  
37 endogenous hormones [1,2]. Several industrial additives suspect of acting as endocrine disruptors  
38 are massively used in food and beverage commodities as well as in personal care products. Among  
39 them, parabens are ubiquitous in cosmetics and toiletries like tooth pastes, deodorants, beauty  
40 creams, solar filters, and bath gels [3-5].

41        Parabens are esters of *p*-hydroxybenzoic acid (*p*-HBA) routinely added as industrial  
42 preservatives due to their antibacterial and antifungal properties. They are characterized by their  
43 low volatility and high stability, liposolubility and hydrophilicity, which together promote their  
44 facile absorption as well as their efficient dispersion and bioaccumulation in the environment [6].  
45 Therefore, concerns have been raised on safety of parabens and its metabolites owing to their  
46 environmental effects [7] as well as their role as endocrine disruptors and their association with  
47 human cancers and allergic contact dermatitis [8-12], although this is still controversial [13]. As a  
48 result, they are banned or restricted, as regulated by the Cosmetic Directive announced in the  
49 [Official Journal of the European Union](#) [14], and paraben-free labels are popping up on beauty  
50 products recently.

51        Due to their widespread use, parabens have been routinely found in water, soil, sediment and  
52 fish [15]. In particular, they are found in samples from wastewater treatment facilities, being  
53 methylparaben (MeP) and *p*-HBA the dominant pollutants [16]. Although many current plants are  
54 thought to remove a large percentage of parabens from aqueous phase, it is unclear if a certain  
55 amount is discharged with the effluent. Overall, there exists a lack of information on the behavior of  
56 parabens during advanced water treatment. Based on such uncertainty, along with the ever  
57 increasing water deficit and demand, continuous development and optimization of highly reliable  
58 water reclamation technologies is mandatory. Although several technologies have been

59 satisfactorily tested for the removal of organic pollutants from water, the advanced oxidation  
60 processes (AOPs) have shown the largest detoxification ability thanks to the production of a very  
61 powerful oxidant like hydroxyl radical ( $\bullet\text{OH}$ ) on site. Some of these AOPs have been scaled-up  
62 with great success, like UV/ $\text{H}_2\text{O}_2$  from Trojan Technologies and conventional Fenton process [17].  
63 In contrast, the use of their electrochemical counterparts (EAOPs) is much more incipient, thereby  
64 requiring further fundamental studies to reach their complete optimization before adapting them to  
65 full-scale systems.

66 Electro-oxidation (EO) has been the most developed EAOP for treating organic pollutants so  
67 far, due to its simplicity combined with high performance [18]. In such cases, adsorbed hydroxyl  
68 radical is formed on the anode surface (M) from water oxidation as shown in reaction (1). In the  
69 presence of  $\text{Cl}^-$ , the concomitant formation of active chlorine ( $\text{Cl}_2/\text{HClO}/\text{ClO}^-$ ) as oxidant occurs in  
70 the bulk from reaction (2). Other reactive species like chlorinated radicals ( $\text{ClOH}\bullet^-$ ,  $\text{Cl}_2\bullet^-$  and  $\text{Cl}\bullet$ )  
71 may be simultaneously formed [19]. Oxidants like  $\text{O}_3$  and  $\text{S}_2\text{O}_8^{2-}$  can also be formed in the bulk  
72 from  $\text{O}_2$  and sulfate oxidation at the anode [18].



75 The most investigated anode materials for decontamination have been boron-doped diamond  
76 (BDD) [20-24], Pt [22,25,26], dimensionally stable anodes (DSA<sup>®</sup>) with either  $\text{IrO}_2$  [22,27-29] or  
77  $\text{RuO}_2$  [30-32] active layers,  $\text{PbO}_2$  [33] and  $\text{SnO}_2$  [18], although less attention has been paid to the  
78 latter two due to problems related to lead leaching and short service life, respectively.

79 If the electrolytic cell incorporates a carbonaceous air-diffusion cathode, which has large ability  
80 to generate  $\text{H}_2\text{O}_2$  as additional oxidant from  $\text{O}_2$  reduction, the process is so-called EO- $\text{H}_2\text{O}_2$  [34].  
81 The performance of this method is greatly enhanced in the presence of  $\text{Fe}^{2+}$  ions at  $\text{pH} \sim 3.0$ , since  
82 hydroxyl radicals can also be formed in the bulk from Fenton's reaction (3). Further enhancement is  
83 reached under UVA irradiation because photolytic reactions yield an extra amount of  $\bullet\text{OH}$ , allow

84 the continuous  $\text{Fe}^{2+}$  regeneration and lead to photodecarboxylation of refractory complexes of  
85 aliphatic by-products. The extraordinary results obtained under the so-called electro-Fenton (EF)  
86 and photoelectro-Fenton (PEF) conditions, respectively, have been demonstrated for several organic  
87 pollutants [35-41].



89 Some authors have compared the performance of the EAOPs upon use of different anodes in  
90 various aqueous media. For example, BDD, Pt,  $\text{IrO}_2$ -based and/or  $\text{RuO}_2$ -based anodes have been  
91 use to degrade naproxen in perchlorate [42], phenanthrene and ranitidine in sulfate [22,43], and  
92 dyes like Acid Red 14 and Rhodamine in various electrolytes [44,45]. But, studies on the  
93 performance of at least two anodes in various electrolytes are more rare [26,46]. A complete  
94 investigation comparing the performance of the four main anodes in  $\text{Cl}^-$  and  $\text{Cl}^-$ -free media is then  
95 needed, with a view toward the application to treatment of real water, where chloride and sulfate are  
96 major anions.

97 This work addresses the degradation of aqueous solutions of MeP at pH 3.0 by EO- $\text{H}_2\text{O}_2$ , EF  
98 and PEF. The electrochemical trials were conducted in undivided tank reactors equipped with an air  
99 diffusion cathode at constant current density ( $j = 66.7 \text{ mA cm}^{-2}$ ) in media containing  $158 \text{ mg L}^{-1}$   
100 MeP in  $\text{Na}_2\text{SO}_4$ ,  $\text{NaCl}$  or  $\text{Na}_2\text{SO}_4 + \text{NaCl}$  as electrolyte. The performance of the three EAOPs using  
101 BDD, Pt,  $\text{IrO}_2$ -based and/or  $\text{RuO}_2$ -based anodes was compared from the analysis of mineralization  
102 profiles and decay kinetics. Primary and final reaction by-products were identified by  
103 chromatographic techniques. To date, only two studies have reported the electrochemical  
104 degradation of MeP in sulfate medium, focusing on its conversion to various by-products in EO  
105 with BDD at very low  $j$  [47,48]. Previous research also assessed the treatment of MeP by  
106 conventional Fenton and UV-driven AOPs [49]. However, Fenton process was inefficient for MeP  
107 degradation, whereas UV-based methods like photo-Fenton yielded better but still partial  
108 conversion values. In contrast, solar photocatalysis with Aeroxide  $\text{TiO}_2$  P-25 was able to completely

109 remove 1 and 10 mg L<sup>-1</sup> MeP from water after 35 and 240 min, respectively [50], but, under the  
110 latter conditions, only 42% mineralization was attained and 6 products were identified. A larger  
111 TOC removal of 80% at 360 min was reported by conventional UV photocatalysis [51]. Several  
112 degradation products, with hydroxylation as major transformation route, were also found upon  
113 ozonation of various parabens including MeP [52].

## 114 **2. Materials and methods**

### 115 *2.1. Chemicals*

116 MeP with  $\geq 99\%$  purity was supplied by Sigma-Aldrich. Anhydrous sodium sulfate and sodium  
117 chloride, used as supporting electrolytes, and iron(II) sulfate heptahydrate, used as catalyst in EF  
118 and PEF, were of analytical grade from Fluka and Sigma-Aldrich. Analytical grade perchloric acid  
119 from Merck was used to regulate the solution pH. Organic solvents, carboxylic acids and other  
120 chemicals were of HPLC or analytical grade from Sigma-Aldrich and Panreac. All the solutions  
121 were prepared with ultrapure water from a Millipore Milli-Q system (resistivity  $>18$  M $\Omega$  cm).

### 122 *2.2. Electrolytic systems*

123 The electrolytic treatments were conducted in an open, undivided, cylindrical, water-jacketed  
124 glass cell containing 100 mL of solution vigorously stirred with a magnetic bar at 800 rpm. The cell  
125 was equipped with a 3 cm<sup>2</sup> anode and a 3 cm<sup>2</sup> carbon-PTFE air-diffusion cathode from E-TEK  
126 (Somerset, NJ, USA), separated about 1 cm. The cathode was mounted as described elsewhere [38]  
127 and was fed with air pumped at 1 L min<sup>-1</sup> for H<sub>2</sub>O<sub>2</sub> generation. Four anode materials were  
128 employed: (i) a BDD thin-film electrode, deposited onto *p*-Si, from NeoCoat, (ii) a Pt sheet  
129 (99.99% purity) from SEMPSA, (iii) a DSA<sup>®</sup>-O<sub>2</sub> plate (IrO<sub>2</sub>-based anode) from NMT Electrodes  
130 and (iv) a DSA<sup>®</sup>-Cl<sub>2</sub> plate (RuO<sub>2</sub>-based anode) from NMT Electrodes. In most of the EF and PEF  
131 trials, 0.50 mM Fe<sup>2+</sup> was added as catalyst because it was found optimal for analogous treatments of  
132 other organic contaminants [37]. All trials were carried out at constant *j* provided by an Agilent

133 6552A (0-25 A, 0-20 V) DC power supply that directly provided the potential difference between  
134 electrodes. For PEF, a Philips TL/6W/08 fluorescent black light blue tube placed 7 cm above the  
135 solution was used, emitting UVA light at  $\lambda_{\max} = 360$  nm with a photoionization energy of  $5 \text{ W m}^{-2}$ ,  
136 measured on a Kipp&Zonen CUV 5 radiometer.

137 Solutions with  $158 \text{ mg L}^{-1}$  MeP ( $1.04 \text{ mM MeP}$ ,  $100 \text{ mg L}^{-1}$  TOC) in different media at pH 3.0,  
138 initially adjusted with  $\text{HClO}_4$ , were comparatively treated at  $35 \text{ }^\circ\text{C}$  and  $j = 66.7 \text{ mA cm}^{-2}$ . This  
139 current density was selected for comparison since it allowed an almost total mineralization upon  
140 PEF within a reasonable time period, as will be discussed below. Three different media with the  
141 same specific conductivity ( $7.40\text{-}7.60 \text{ mS cm}^{-1}$ ) were tested as background electrolyte:  $0.050 \text{ M}$   
142  $\text{Na}_2\text{SO}_4$ ,  $0.070 \text{ M NaCl}$  and  $0.025 \text{ M Na}_2\text{SO}_4 + 0.035 \text{ M NaCl}$ . Note that a high MeP concentration  
143 was chosen in order to assess the mineralization rate of each system. Before the assays, cleaning of  
144 the anode and activation of the cathode were ensured under polarization in  $0.050 \text{ M Na}_2\text{SO}_4$  at  $100$   
145  $\text{mA cm}^{-2}$  for 180 min.

### 146 *2.3. Apparatus and analytical procedures*

147 The solution pH and conductance were determined with a Crison 2000 pH-meter and a  
148 Metrohm 644 conductometer, respectively. The  $\text{H}_2\text{O}_2$  concentration accumulated from cathodic  $\text{O}_2$   
149 reduction was obtained from the absorbance of the titanous-hydrogen peroxide colored complex at  $\lambda$   
150  $= 408 \text{ nm}$  [53], using a Shimadzu 1800 UV/Vis spectrophotometer at  $35 \text{ }^\circ\text{C}$ . The active chlorine  
151 produced in experiments carried out in the presence of  $\text{Cl}^-$  was determined by the *N,N*-diethyl-*p*-  
152 phenylenediamine (DPD) colorimetric method according to Standard Methods [54]. To do this, the  
153 same spectrophotometer was set at  $\lambda = 515 \text{ nm}$ . For total organic carbon (TOC) analysis, samples  
154 were withdrawn from raw and treated solutions, filtered with  $0.45 \text{ }\mu\text{m}$  PTFE filters from Whatman  
155 and directly injected into a Shimadzu VCSN TOC analyzer.

156 Assuming the following reaction for total mineralization of MeP:



158 the mineralization current efficiency (MCE) values for each trial were estimated as follows [44,55]:

159

$$160 \text{ MCE (\%)} = \frac{n F V \Delta(\text{TOC})_{\text{exp}}}{4.32 \times 10^7 m I t} \times 100 \quad (5)$$

161 where  $n = 34$  is the number of electrons for the mineralization,  $F$  is the Faraday constant (96,487 C  
162  $\text{mol}^{-1}$ ),  $V$  is the solution volume (L),  $\Delta(\text{TOC})_{\text{exp}}$  is the experimental TOC decay ( $\text{mg C L}^{-1}$ ),  $4.32 \times$   
163  $10^7$  is a conversion factor to homogenize the units ( $3600 \text{ s h}^{-1} \times 12,000 \text{ mg C mol}^{-1}$ ),  $m = 8$  is the  
164 number of carbon atoms of MeP,  $I$  is the applied current (A) and  $t$  is the electrolysis time (h).

165 The specific energy consumption per unit TOC mass ( $\text{EC}_{\text{TOC}}$ ) was estimated as follows [44]:

$$166 \text{ EC}_{\text{TOC}} (\text{kWh (g TOC)}^{-1}) = \frac{E_{\text{cell}} I t}{V_s \Delta(\text{TOC})_{\text{exp}}} \quad (6)$$

167 where  $E_{\text{cell}}$  is the potential difference of the cell (V) and the rest of parameters have been already  
168 defined. The average  $E_{\text{cell}}$  values were 15.0 V for EAOPs with BDD and 12.5 V with the other three  
169 anodes.

170 The decay kinetics of MeP was determined by analyzing the degraded solutions by reversed-  
171 phase high-performance liquid chromatography (HPLC) through a Waters 600 LC fitted with a  
172 BDS Hypersil C18 6  $\mu\text{m}$ , 250 mm  $\times$  4.6 mm, column at 35  $^{\circ}\text{C}$  and coupled to a Waters 996  
173 photodiode array detector set at  $\lambda = 258 \text{ nm}$ . In the EF and PEF experiments, the aqueous samples  
174 were diluted with the same volume of acetonitrile to stop the degradation process. These  
175 measurements were made by injecting 20  $\mu\text{L}$  aliquots into the LC after microfiltration with the 0.45  
176  $\mu\text{m}$  PTFE filters using a 40:60 (v/v) acetonitrile/water mixture at 1  $\text{mL min}^{-1}$  as mobile phase. The  
177 chromatograms displayed a well-defined peak related to MeP at retention time ( $t_r$ ) of 5.2 min.

178 Short-chain linear carboxylic acids were detected by ion-exclusion HPLC using a Waters 600  
179 LC fitted with a Bio-Rad Aminex HPX 87H, 300 mm  $\times$  7.8 mm, column at 35  $^{\circ}\text{C}$  and coupled to a  
180 Waters 996 photodiode detector selected at  $\lambda = 210 \text{ nm}$ . A 4 mM  $\text{H}_2\text{SO}_4$  solution eluted at 0.6 mL  
181  $\text{min}^{-1}$  was used as mobile phase. An absorption peak appeared at  $t_r$  of 6.7 min related to oxalic acid.

182 To enhance the identification of aromatic and aliphatic intermediates in the presence and  
183 absence of  $\text{Cl}^-$ , various samples were withdrawn during short treatments of MeP solutions in 0.050  
184 M  $\text{Na}_2\text{SO}_4$  or 0.025 M  $\text{Na}_2\text{SO}_4$  + 0.035 M  $\text{NaCl}$  at pH 3.0. The treated solutions were lyophilized,  
185 the organic components were extracted with  $\text{CH}_2\text{Cl}_2$  and ethyl acetate, and then the supernatant was  
186 concentrated up to ca. 1 mL with  $\text{N}_{2(\text{g})}$  to be analyzed by gas chromatography-mass spectrometry  
187 (GC-MS). This was made with an Agilent Technologies system composed of a 6890N gas  
188 chromatograph equipped with a 7683B series injector and coupled to a 5975XL mass spectrometer  
189 operating in electron ionization mode at 70 eV. A nonpolar Teknokroma Sapiens-X5 ms capillary  
190 column, 0.25  $\mu\text{m}$ , 30 m  $\times$  0.25 mm, was used. The temperature ramp was: 36  $^\circ\text{C}$  for 1 min, 5  $^\circ\text{C}$   
191  $\text{min}^{-1}$  up to 320  $^\circ\text{C}$ , and hold time of 10 min. The temperature of the inlet, source and transfer line  
192 was 250, 230 and 280  $^\circ\text{C}$ . The analysis was made by splitless (0.7 min) injection mode. Masses  
193 ranging from 50 to 550 units ( $m/z$ ) were analyzed, employing a NIST05 MS library to identify the  
194 mass spectra.

### 195 **3. Results and discussion**

#### 196 *3.1. Mineralization of methylparaben solutions in different media using BDD, Pt and DSA*

197 A series of electrolytic trials was carried out in the absence and presence of MeP at  $j = 66.7$  mA  
198  $\text{cm}^{-2}$  in pure  $\text{Na}_2\text{SO}_4$  (0.050 M), pure  $\text{NaCl}$  (0.070 M) and a  $\text{Cl}^-/\text{SO}_4^{2-}$  mixture (0.025 M  $\text{Na}_2\text{SO}_4$  +  
199 0.035 M  $\text{NaCl}$ ). Preliminary tests were performed in the raw electrolytes aiming to quantify the  
200 concentration of active chlorine and/or  $\text{H}_2\text{O}_2$  accumulated in the bulk from direct  $\text{Cl}^-$  oxidation at  
201 the anode and  $\text{O}_2$  reduction at the cathode, respectively. First, the optimization of the amount of  
202  $\text{Fe}^{2+}$  added as catalyst to the solution in the Fenton-based EAOPs was done through a series of  $\text{H}_2\text{O}_2$   
203 electrogeneration experiments by EF with a BDD anode in  $\text{Na}_2\text{SO}_4$  at pH 3.0. As shown in Fig. S1,  
204 the concentration of  $\text{H}_2\text{O}_2$  reached a plateau after a given electrolysis time in all the 0.15-1.00 mM  
205  $\text{Fe}^{2+}$  range, when its production and destruction rates equated. A lower steady state content was

206 attained when increasing the  $\text{Fe}^{2+}$  concentration, due to the progressively greater destruction of  
207  $\text{H}_2\text{O}_2$  from Fenton's reaction (3). The minimum steady content at 360 min was 26 mM  $\text{H}_2\text{O}_2$ ,  
208 attained at 0.50 mM  $\text{Fe}^{2+}$ , whereas greater iron concentrations enhanced the accumulation up to 44  
209 mM  $\text{H}_2\text{O}_2$ . The behavior at 0.50 mM  $\text{Fe}^{2+}$  can thus be explained by the efficient reaction between  
210 both Fenton's reagents, yielding the largest amount of  $\bullet\text{OH}$  from reaction (3). This oxidant would  
211 then be readily available for decontamination in the presence of organic pollutants, whereas the  
212 presence of an excess of  $\text{Fe}^{2+}$  ions would be detrimental because of the partial consumption of  $\bullet\text{OH}$   
213 in parasitic reactions.

214 Once optimized the  $\text{Fe}^{2+}$  content, the effect of chloride ion on the  $\text{H}_2\text{O}_2$  electrogeneration was  
215 investigated by electrolyzing the raw  $\text{Cl}^-/\text{SO}_4^{2-}$  mixture with 0.50 mM  $\text{Fe}^{2+}$  at pH 3.0 under EF  
216 conditions with BDD. As observed in Fig. 1, the steady  $\text{H}_2\text{O}_2$  concentration at 360 min was about  
217 half the value attained in the absence of chloride (see Fig. S1), which means that in the mixture  
218  $\text{H}_2\text{O}_2$  not only disappears due to Fenton's reaction but to some additional reagent that causes its  
219 destruction. Fig. 1 reveals the accumulation of active chlorine, which attained a steady value of 7.2  
220  $\text{mg L}^{-1}$  from 180 min. Therefore, the additional destruction of  $\text{H}_2\text{O}_2$  may be accounted for by its  
221 reaction with  $\text{HClO}$  [44]:



223 The presence of chloride ion is detrimental in terms of  $\bullet\text{OH}$  formation in the bulk, not only  
224 indirectly from reaction (7), but also due to the direct destruction of this oxidizing radical ( $\bullet\text{OH}$   
225 and/or  $\text{M}(\bullet\text{OH})$ ) as follows [44]:



227 The bright side in the mixture would be thus related to the formation of radicals like  $\text{Cl}\bullet$  (as  
228 well as  $\text{ClOH}\bullet^-$  and  $\text{Cl}_2\bullet^-$ ) and, mainly, the accumulation of active chlorine, which may act as an  
229 oxidant. In Fenton-based systems like EF performed in the presence of chloride, reactivity of

230 oxidizing species presents some particularity. Indeed,  $\bullet\text{OH}$  can also be formed in the bulk from  
231 Fenton-like reaction between active chlorine (assuming the role of  $\text{H}_2\text{O}_2$ ) and iron ions [56,57]:



233 Note that [26] reported the accumulation of a much greater active chlorine concentration, up to  
234 7 mM, upon electrolysis of a 0.05 M NaCl solution by EO with a BDD/stainless steel cell at 100  
235  $\text{mA cm}^{-2}$ . This supports the active role of  $\text{H}_2\text{O}_2$  and  $\text{Fe}^{2+}$  in the disappearance of HClO by reactions  
236 like (7) and (9) under the tested conditions.

237 Once clarified the ability of these systems to produce  $\text{H}_2\text{O}_2$  and active chlorine, as well as the  
238 role of these species in the formation of  $\bullet\text{OH}$  in the bulk, solutions of  $158 \text{ mg L}^{-1}$  MeP in each of the  
239 three media at pH 3.0 were treated by EO- $\text{H}_2\text{O}_2$  (no iron), as well as by EF and PEF ( $0.5 \text{ mM Fe}^{2+}$ ).  
240 Fig. 2a illustrates the comparative performance of the three EAOPs with a BDD anode using the  
241  $\text{Cl}^-/\text{SO}_4^{2-}$  mixture. A gradual TOC abatement with 89.0% removal at 360 min was achieved in EO-  
242  $\text{H}_2\text{O}_2$  owing to the combined action of BDD( $\bullet\text{OH}$ ) and active chlorine on MeP and its reaction  
243 intermediates. EF yielded a very similar trend, with only 3%-7% larger mineralization at each given  
244 time and a final TOC abatement of 91%. The slightly better results may be explained by the  
245 formation of  $\bullet\text{OH}$  in the bulk from Fenton's reaction (3). However, its concentration is reduced as a  
246 result of the large destruction of  $\text{H}_2\text{O}_2$  from reaction (7), despite the simultaneous co-generation  
247 from Fenton-like reaction (9). The formation of chloroderivatives and refractory complexes  
248 between Fe(III) and some by-products, which are hardly oxidizable by the low amount of available  
249  $\bullet\text{OH}$ , is responsible for the similarity between EO- $\text{H}_2\text{O}_2$  and EF at 360 min. In contrast, a  
250 significantly quicker and larger TOC removal was achieved by PEF, reaching 97% mineralization.  
251 This means that this EAOP is powerful enough to progressively degrade MeP and all the refractory  
252 by-products, either uncomplexed or complexed with  $\text{Fe}^{3+}$ . UVA radiation allows: (i) the continuous  
253 regeneration of  $\text{Fe}^{2+}$  from Fe(III) photoreduction, thus enhancing the production of  $\bullet\text{OH}$  in the bulk

254 from reactions (3) and (9), and (ii) the photodecarboxylation of persistent complexes, which  
255 upgrades the TOC removal and regenerates  $\text{Fe}^{2+}$  as well [34,38].

256 The influence of the anode material on the performance of the EAOPs is shown in Fig. 2b. In  
257 EO- $\text{H}_2\text{O}_2$ , the use of  $\text{IrO}_2$ -based, Pt and  $\text{RuO}_2$ -based anodes led to a rather poor mineralization at  
258 360 min, being much larger with the latter two anodes (43%) than with the former one (1.9%). This  
259 behavior arises from the lower oxidation power of  $\text{IrO}_2(\bullet\text{OH})$ ,  $\text{Pt}(\bullet\text{OH})$  and  $\text{RuO}_2(\bullet\text{OH})$  formed from  
260 reaction (1) compared to  $\text{BDD}(\bullet\text{OH})$ , since they are chemisorbed rather than physisorbed radicals.  
261 The superiority of the Pt and  $\text{RuO}_2$ -based anodes compared to the  $\text{IrO}_2$ -based one may arise from  
262 the larger  $\text{O}_2$ -evolution overpotential of Pt and the great ability of the  $\text{RuO}_2$ -based anode to produce  
263 active chlorine [58]. On the other hand, the trends in PEF with these three anodes were much more  
264 similar, with 85% TOC removal using the  $\text{RuO}_2$ -based anode and 89%-91% with the other ones.  
265 The larger production of active chlorine with the former anode causes a higher destruction of  $\text{H}_2\text{O}_2$   
266 from reaction (7) and results in a poorer concentration of  $\bullet\text{OH}$  in the bulk, which justifies the lower  
267 oxidation power. In conclusion, PEF with BDD was the optimum process in the  $\text{Cl}^-/\text{SO}_4^{2-}$  medium  
268 as a result of the best balance between active chlorine,  $\bullet\text{OH}$  and  $\text{M}(\bullet\text{OH})$  formed as main oxidants.  
269 These species, along with UVA photons, ensured the almost total degradation of refractory by-  
270 products. However, the systems equipped with BDD have to be carefully optimized because,  
271 otherwise, toxic  $\text{ClO}_4^-$  may be formed, as reported during the electrochemical oxidation of  $\text{Cl}^-$  at  
272 this anode [59-61], which occurs to a lower extent using less oxidant ones like Pt [61].

273 Fig. 3a depicts the comparative TOC-time trends for the different EAOPs with BDD in  
274  $\text{Na}_2\text{SO}_4$ . A slower mineralization, reaching a final value of 77%, was found in EO- $\text{H}_2\text{O}_2$  from the  
275 main action of  $\text{BDD}(\bullet\text{OH})$ . The synergistic occurrence of active chlorine in the previous  $\text{Cl}^-/\text{SO}_4^{2-}$   
276 mixture was thus beneficial to attain a larger TOC abatement, although in that medium the final  
277 solution probably contained a certain number of toxic, chlorinated by-products. In contrast, the  
278 mineralization percentages at 360 min in EF and PEF (89% and 97%, respectively) were very close

279 to those achieved in the presence of chloride ion. This means that  $\bullet\text{OH}$  formed in the bulk are highly  
280 effective for degrading the chlorinated derivatives in the  $\text{Cl}^-/\text{SO}_4^{2-}$  mixture. Nevertheless, note that  
281 the TOC removal rates were somewhat higher in  $\text{Na}_2\text{SO}_4$ . For example, at 180 min of EF and PEF,  
282 the mineralization was 78% and 92% (see Fig. 3a) instead of 69% and 80% (see Fig. 2a), which  
283 confirms the slower accumulation of  $\bullet\text{OH}$  and  $\text{M}(\bullet\text{OH})$  in the presence of chloride ion due to  
284 parasitic reactions. The same occurred in PEF with Pt,  $\text{IrO}_2$ -based and  $\text{RuO}_2$ -based anodes, since  
285 significantly greater TOC abatements were attained at any given time up to reach 98%  
286 mineralization at 360 min in all cases (see Fig. 3b). The quicker and larger TOC decay compared to  
287 that in  $\text{Cl}^-$ -containing medium, along with the almost identical profiles of the four PEF treatments  
288 in  $\text{Na}_2\text{SO}_4$ , allows inferring the preponderant role of homogeneous  $\bullet\text{OH}$  over  $\text{M}(\bullet\text{OH})$  in the latter  
289 medium, as well as their lower destruction by parasitic reactions. Fig. 3b also shows the very poor  
290 performance of  $\text{EO-H}_2\text{O}_2$  with the three anodes, attaining 6.9%-8.5% with DSA ones and 17% with  
291 Pt. These results are worse than those obtained with either BDD (see Fig. 3a) or with the same three  
292 anodes in the  $\text{Cl}^-/\text{SO}_4^{2-}$  mixture (see Fig. 2b), which confirms the low oxidation power of the  
293  $\text{M}(\bullet\text{OH})$  (especially the  $\text{DSA}(\bullet\text{OH})$ ) formed on their surface compared to  $\text{BDD}(\bullet\text{OH})$  and the  
294 consequent importance of active chlorine contribution to oxidation in those cases. Hence, PEF with  
295 a low cost anode like DSA is the treatment of choice in  $\text{Cl}^-$ -free medium like sulfate, since  $\bullet\text{OH}$   
296 formed in the bulk along with UVA light are the main agents to transform the organic matter into  
297 innocuous by-products.

298 The clear effect of chloride ion on mineralization was confirmed by comparing the trends of  
299  $\text{EO-H}_2\text{O}_2$ , EF and PEF with BDD in pure  $\text{NaCl}$  shown in Fig. 4. It can be seen that, as expected, the  
300 oxidation power increased in the order:  $\text{EO-H}_2\text{O}_2 < \text{EF} < \text{PEF}$ . However, the presence of chloride  
301 ion and the formation of active chlorine unified the degradation results at long electrolysis time,  
302 yielding 86%, 90% and 93% at 360 min, respectively. These values confirm the positive  
303 contribution of chloride in  $\text{EO-H}_2\text{O}_2$ , as compared with Fig. 3a, whereas in EF and PEF this anion

304 leads to slightly slower mineralization rates and/or final TOC abatements. Despite this deceleration  
305 in the presence of chloride, a large decontamination was achieved again by PEF.

306 Several authors have recently reported interesting results on other EAOPs such as electro-  
307 peroxone [62] and photoelectro-peroxone [63,64], which involve the generation of  $\bullet\text{OH}$  from  
308 injected  $\text{O}_3$  and electrogenerated  $\text{H}_2\text{O}_2$  at a carbonaceous cathode and/or the photolysis of the latter  
309 species upon UVC irradiation. During the treatment of benzene derivatives and 1,4-dioxane, no  
310 significant influence of the anode nature (Ti/Pt, Ti/RuO<sub>2</sub>-IrO<sub>2</sub> and BDD) on TOC removal was  
311 found in sulfate medium, owing to the high oxidation power of  $\text{O}_3$  on  $\bullet\text{OH}$  generation. In contrast,  
312 in  $\text{Cl}^-$  medium, a strong inhibition of mineralization was observed due to the removal of  $\text{H}_2\text{O}_2$  with  
313 generated  $\text{HClO}$  from reaction (7), which was more significant using a DSA anode owing to its  
314 larger production of active chlorine. The addition of  $\text{Fe}^{2+}$  to the solution caused a decrease in  
315 mineralization rate in electro-peroxone, being related to the formation of Fe(III)-carboxylate  
316 complexes, but in photoelectro-peroxone such species were photolyzed by UVC light [64].

### 317 *3.2. Mineralization current efficiency and energy consumption*

318 The MCE and  $\text{EC}_{\text{TOC}}$  values corresponding to the TOC-time profiles presented in Fig. 2-4 were  
319 calculated using Eq. (5) and (6), respectively. Fig. 5 illustrates the MCE curves obtained in the  
320  $\text{Cl}^-/\text{SO}_4^{2-}$  mixture, which resulted from TOC trends of Fig. 2. As can be seen in Fig. 5a, at any  
321 given time, the current efficiency with BDD increased in agreement with the larger oxidation power  
322 in the order:  $\text{EO-H}_2\text{O}_2 < \text{EF} < \text{PEF}$ , since the production of reactive species was accelerated upon  
323 use of  $\text{Fe}^{2+}$  and UVA light. The highest MCE values with this anode were obtained at short  
324 electrolysis time (20-40 min), reaching 11.0%, 15.6% and 17.7%, respectively. Afterwards, the  
325 MCE underwent a progressive decay in all cases up to a final value around 7.0%-7.6% (see Table  
326 1), in accordance with the close TOC values found at 360 min (see Fig. 2a). The current efficiency  
327 fall over time can be accounted for by: (i) the increasing mass transport limitations due to organic  
328 matter removal, which enhances the role of parasitic reactions involving the reactive species, and

329 (ii) the formation of more hardly degradable by-products, including chlorinated derivatives and  
330 Fe(III) complexes with short aliphatic compounds [18,44]. All these findings were confirmed using  
331 Pt, IrO<sub>2</sub>-based and RuO<sub>2</sub>-based anodes. As shown in Fig. 5b, PEF was much more efficient than  
332 EO-H<sub>2</sub>O<sub>2</sub>, especially at short time with MCE values of ~ 20% and < 10%, respectively. The current  
333 efficiency of the three PEF treatments was analogous to that of PEF with BDD (see Table 1),  
334 whereas the EO-H<sub>2</sub>O<sub>2</sub> treatments were less efficient than that with BDD during all the electrolysis  
335 time. Table 1 summarizes the MCE values obtained at 360 min by EO-H<sub>2</sub>O<sub>2</sub>, EF and PEF in  
336 Na<sub>2</sub>SO<sub>4</sub> and NaCl media. Note that a similar current efficiency around 7% was achieved in all the  
337 PEF treatments.

338 Fig. 6a illustrates that, using BDD in the Cl<sup>-</sup>/SO<sub>4</sub><sup>2-</sup> mixture, a higher energy consumption was  
339 required as the oxidation power of the EAOP diminished in the order: PEF < EF < EO-H<sub>2</sub>O<sub>2</sub>, in  
340 correspondence with a less efficient process (see Fig. 5a). Moreover, EC<sub>TOC</sub> always increased over  
341 time up to final values of 1.54-1.86 kWh (g TOC)<sup>-1</sup>. This is reasonable, since constant current and  
342  $E_{\text{cell}}$  were ascertained during the experiments, whereas the gradually lower mineralization rate led to  
343 a more difficult removal of TOC content (see Fig. 2a). Similar trends can be observed in Fig. 6b for  
344 the EAOPs with the other three anodes, with significantly greater energy consumption in EO-H<sub>2</sub>O<sub>2</sub>  
345 due to their lower degradation performance (see Fig. 2b). In particular, very high energy  
346 consumptions were needed when using the RuO<sub>2</sub>-based anode, up to 60 min, because of its small  
347 oxidation power. The EC<sub>TOC</sub> values at 360 min for the trials carried out in Na<sub>2</sub>SO<sub>4</sub> and NaCl are  
348 summarized in Table 1. It can then be concluded that, unless renewable energy is used to power the  
349 systems, the treatments become significantly more expensive at long electrolysis times, but  
350 coupling with less expensive post-treatments can be envisaged to reduce operation expenses.

### 351 3.3. Comparison of MeP decay kinetics

352 The influence of the EAOP and anode nature on the decay of MeP concentration with  
353 electrolysis time was assessed for the previous treatments of solutions containing 158 mg L<sup>-1</sup> of

354 pollutant in each medium at pH 3.0. Fig. 7 shows the decays upon use of BDD in the  $\text{Cl}^-/\text{SO}_4^{2-}$   
355 mixture and the corresponding kinetic analysis when feasible. In EO- $\text{H}_2\text{O}_2$  and EF, MeP  
356 disappeared completely at 120 min. Both trends agree well with a pseudo-first-order reaction, as  
357 shown in the inset, yielding very close apparent rate constants ( $k_1$ ) of  $3.43 \times 10^{-2}$  and  $4.07 \times 10^{-2}$   
358  $\text{min}^{-1}$  in EO- $\text{H}_2\text{O}_2$  and EF, respectively. The existence of such reaction kinetics suggests that MeP  
359 reacts with a constant concentration of reactive species. Based on the poor difference between both  
360 EAOPs, it can be concluded that BDD( $\bullet\text{OH}$ ) and active chlorine act as main oxidants, being the  
361 contribution of  $\bullet\text{OH}$  in the bulk much less relevant. This confirms the comments made for the  
362 mineralization trends of Fig. 2a, with a large amount of the  $\text{H}_2\text{O}_2$  required for Fenton's reaction  
363 being destroyed by  $\text{HClO}$ . In contrast, the profile of the MeP decay in PEF, shown in Fig. 7b,  
364 presented two major differences from those of Fig. 7a: (i) a complex kinetics appeared, not  
365 corresponding to a pseudo-first-order reaction, and (ii) a faster MeP removal was obtained, with a  
366 disappearance of 66% instead of 41% after 10 min. Since MeP was photostable under UVA  
367 irradiation (not shown), these two facts can be explained by the contribution of additional  $\bullet\text{OH}$  in  
368 the bulk. Indeed, the continuous  $\text{Fe}^{2+}$  regeneration thanks to Fe(III) photoreduction enhances the  
369 accumulation of  $\bullet\text{OH}$  from Fenton's reaction (3), as compared to EF. But, even more relevant, such  
370 a great  $\text{Fe}^{2+}$  availability promotes the formation of  $\bullet\text{OH}$  from Fenton-like reaction (9).  
371 Consequently, PEF in the presence of chloride entails a very complex and powerful reaction  
372 environment with multiple oxidants of variable concentration over time. This finding is highly  
373 interesting because, to our knowledge, the decay kinetics of organic pollutants in Fenton-based  
374 EAOPs in chloride medium has not been reported yet, only existing studies that report the effect of  
375 chloride ion on TOC and color removal [26]. The use of Pt and DSA instead of BDD led to similar  
376 MeP decays, with a removal percentage around 60-65% (not shown). This means that, in PEF, the  
377 preponderant oxidizing role corresponded to bulk oxidants (active chlorine and  $\bullet\text{OH}$ ), being less  
378 important the influence of the adsorbed  $\text{M}(\bullet\text{OH})$ .

379 The analogous MeP decays in Na<sub>2</sub>SO<sub>4</sub> depicted in Fig. 8 exhibit significant differences from  
380 those obtained in the electrolyte mixture. The profile in EO-H<sub>2</sub>O<sub>2</sub> was still exponential (see Fig. 8a),  
381 but showing a much slower MeP removal with only 80% of disappearance at 360 min. Accordingly,  
382 a  $k_1 = 4.96 \times 10^{-3} \text{ min}^{-1}$  (one order of magnitude lower compared to results of Fig. 7a) was achieved.  
383 This much slower degradation, with BDD( $\bullet$ OH) as the main oxidant, justifies the decisive  
384 contribution of active chlorine in EO-H<sub>2</sub>O<sub>2</sub> in the Cl<sup>-</sup>/SO<sub>4</sub><sup>2-</sup> mixture (see above). In contrast, Fig. 8b  
385 shows that straight decays were obtained in EF and PEF, with an analogous profile in both cases,  
386 not corresponding to a pseudo-first-order reaction but to a complex kinetics. Furthermore, the  
387 removal of MeP was much faster compared to EO-H<sub>2</sub>O<sub>2</sub>, and was also quicker than any other  
388 EAOP performed in the previous medium. For example, in only 10 min, the MeP content decreased  
389 by 94%. In these cases, the great amount of  $\bullet$ OH produced in the bulk from Fenton's reaction (3),  
390 along with adsorbed M( $\bullet$ OH), is the main responsible for the particular reaction kinetics, without  
391 much influence of UVA light. Interestingly, also the PEF treatments with Pt and DSA led to a  
392 complex kinetics with similar decay rate, with MeP removal at 10 min ranging between 93% and  
393 95% (not shown).

#### 394 *3.4. Elucidation of reaction routes for MeP mineralization*

395 In previous sections, some of the profiles have been explained on the basis of the formation of  
396 specific reaction by-products. A GC-MS analysis of treated solutions was then carried out in order  
397 to identify as many products as possible, aiming to elucidate the preeminent degradation routes.  
398 Since, in a given medium, the same kinds of reactive species contribute to MeP transformation in  
399 all the EAOPs regardless of the anode used, BDD was chosen to perform this thorough study.

400 Table S1 summarizes the characteristics of aromatic and aliphatic intermediates detected during  
401 the degradation of solutions with 158 mg L<sup>-1</sup> MeP in the Cl<sup>-</sup>/SO<sub>4</sub><sup>2-</sup> mixture at pH 3.0. From these  
402 13 by-products, the reaction sequence of Fig. 9 is proposed. MeP (**1**) is transformed into three  
403 different primary aromatic by-products as a result of: (i) direct attack of  $\bullet$ OH or BDD( $\bullet$ OH) to yield

404 a hydroxylated MeP (**2a**), (ii) nucleophilic attack of hydroxyl radicals onto the carbon atom of the  
405 carbonyl group, causing the release of the  $-OCH_3$  group to yield 4-hydroxybenzoic acid (**3a**), and  
406 (iii) chlorination to form a chlorinated MeP (**4a**). Decarboxylation of **3a** upon attack of hydroxyl  
407 radical yields hydroquinone (**11a**), whereas hydroxylation in concomitance of chlorination leads to  
408 several polychlorinated phenols (**5a**, **6a** and **7a**). On the other hand, consecutive action of active  
409 chlorine on **4a** causes its cleavage to yield aliphatic polychlorinated compounds (**8a**, **9a** and **10a**).  
410 These by-products can be mineralized, or may undergo further transformations under the action of  
411 hydroxyl radicals and active chlorine as occurs with the aromatic molecules. Various short-chain  
412 aliphatic carboxylic acids (**12a**, **13a** and **14a**), either complexed with Fe(III) or uncomplexed, are  
413 produced and further converted into  $CO_2$ ,  $Cl^-$  and  $H_2O$ . As shown in Fig. 2a, mineralization of all  
414 these intermediates is almost total in PEF with BDD.

415 An analogous study performed in  $Na_2SO_4$  under the same conditions resulted in the 7 by-  
416 products summarized in Table S2, giving rise to the reaction sequence of Fig. 10. Primary  
417 intermediates **2a** and **3a** are also formed in this medium. In addition, hydroxylation of MeP yields  
418 products **4b** and **5b**, which may end in **6b**. On the other hand, the attack of hydroxyl radicals on the  
419 benzenic C atom of MeP bonded to carbonyl group, or on some of the by-products, yields  
420 hydroquinone (**11a**), which might be further transformed into malonic acid (**7b**) prior to overall  
421 mineralization.

422 These findings agree with recent literature. For example, Steter et al. [47,48] reported the  
423 formation of 4-hydroxybenzoic acid (**3a**) as the first transformation step of MeP by EO with BDD  
424 in  $K_2SO_4$ . This was converted to phenol, and further to hydroquinone (**11a**) and *p*-benzoquinone.  
425 The formation of hydroquinone has also been ascertained in solar photocatalysis [50]. Finally,  
426 during the ozonation of various parabens, **3a** and **11a** were also found as major breakdown products  
427 [52].

428 As observed in Fig. 9 and 10, carboxylic acids were the final by-products before reaching the  
429 total mineralization, as also reported by Steter [48]. HPLC analysis revealed that the greatest  
430 accumulation corresponded to oxalic acid, attaining 17, 30 and 42 mg L<sup>-1</sup> as maximal in EO-H<sub>2</sub>O<sub>2</sub>,  
431 EF and PEF with BDD in Na<sub>2</sub>SO<sub>4</sub>, respectively (see Fig. 11a). An almost total removal was  
432 achieved at 360 min in PEF thanks to photodecarboxylation of Fe(III)-oxalate complexes under  
433 UVA irradiation [38], in agreement with the overall mineralization shown in Fig. 3a, whereas the  
434 acid was more refractory to attack by BDD(<sup>•</sup>OH) and <sup>•</sup>OH in EO-H<sub>2</sub>O<sub>2</sub> and EF, respectively. In  
435 PEF with chloride ion, a much lower content of oxalic acid was attained, being further mineralized.  
436 Finally, it can be noted in Fig. 11b that PEF with Pt and DSA in Na<sub>2</sub>SO<sub>4</sub> led to very similar profiles  
437 and values of oxalic acid, also close to those obtained with BDD, which agrees with the TOC-time  
438 trends commented from Fig. 3b, corroborating the powerful action of UVA irradiation onto its  
439 Fe(III) complexes.

#### 440 **4. Conclusions**

441 Different anode materials may be used for degrading MeP by EAOPs, being the selection  
442 dependent on the background electrolyte contained in the water matrix. If the aim is simply  
443 reaching a quick decay kinetics of the parent pollutant, PEF with DSA is the system of choice in  
444 either absence or presence of chloride ion, since it performs like PEF with BDD or Pt but DSA is  
445 much less expensive. In all media, PEF led to a complex decay kinetics, with <sup>•</sup>OH from Fenton's  
446 reaction as the main reactive species in Na<sub>2</sub>SO<sub>4</sub>, and active chlorine plus <sup>•</sup>OH from Fenton-like  
447 reaction between Fe<sup>2+</sup> and HClO as the preeminent reactive species in the Cl<sup>-</sup>/SO<sub>4</sub><sup>2-</sup> mixture.  
448 Otherwise, if a large mineralization percentage is aimed, PEF with BDD must be chosen in the  
449 presence of chloride ion, whereas a less expensive PEF with DSA is enough in the absence of this  
450 anion. PEF trials presented a higher MCE and lower EC<sub>TOC</sub> than EF and EO-H<sub>2</sub>O<sub>2</sub> due to its larger  
451 oxidation power. Up to 13 by-products were identified in the Cl<sup>-</sup>/SO<sub>4</sub><sup>2-</sup> mixture, including

452 chlorinated and non-chlorinated ones, and 7 molecules were found in Na<sub>2</sub>SO<sub>4</sub>, with oxalic acid as  
453 major final short-chain aliphatic acid prior to overall mineralization of MeP.

#### 454 **Acknowledgments**

455 Financial support from project CTQ2013-48897-C2-1-R (MINECO/FEDER, EU) is  
456 acknowledged. J. R. Steter thanks funding from process number 234142/2014-6 (CNPq, Brazil).

457 **References**

- 458 [1] S.M. Dickerson, A.C. Gore, Estrogenic environmental endocrine-disrupting chemical effects on  
459 reproductive neuroendocrine function and dysfunction across the life cycle, Rev. Endocr.  
460 Metab. Disord. 8 (2007) 143-159.
- 461 [2] E. Diamanti-Kandarakis, J.P. Bourguignon, L.C. Giudice, R. Hauser, G.S. Prins, A.M. Soto,  
462 R.T. Zoeller, A.C. Gore, Endocrine-disrupting chemicals: an Endocrine Society scientific  
463 statement, Endocr. Rev. 30 (2009) 293-342.
- 464 [3] F.A. Andersen, Final amended report on the safety assessment of methyl paraben, ethyl paraben,  
465 propyl paraben, and benzyl paraben as used in cosmetic products, Int. J. Toxicol. 27 (2008) 1-  
466 82.
- 467 [4] Y. Guo, K. Kannan, A survey of phthalates and parabens in personal care products from the  
468 United States and its implications for human exposure, Environ. Sci. Technol. 47 (2013)  
469 14442-14449.
- 470 [5] Y. Guo, L., Kannan, A survey of phthalates and parabens in personal care products from the  
471 United States and its implications for human exposure, Environ. Sci. Technol. 47 (2013)  
472 14442-14449.
- 473 [6] C. Haman, X. Dauchy, C. Rosin, J.-F. Munoz, Occurrence, fate and behavior of parabens in  
474 aquatic environments: A review, Water Res. 68 (2015) 1-11.
- 475 [7] D. Błędzka, J. Gromadzińska, W. Wasowicz, Parabens. From environment studies to human  
476 health, Environ. Int. 67 (2014) 27-42.
- 477 [8] P.D. Darbre, A. Aljarrah, W.R. Miller, N.G. Coldham, M.J. Sauer, G.S. Pope, Concentrations of  
478 parabens in human breast tumor, J. Appl. Toxicol. 24 (2004) 5-13.
- 479 [9] P.W. Harvey, D.J. Everett, Significance of the detection of esters of *p*-hydroxybenzoic acid  
480 (parabens) in human breast tumours, J. Appl. Toxicol. 24 (2004) 1-4.

- 481 [10] M.G. Soni, I.G. Carabin, G.A. Buradock, Safety assessment of esters of *p*-hydroxybenzoic acid  
482 (parabens), Food Chem. Toxicol. 43 (2005) 985-1015.
- 483 [11] J. Boberg, C. Taxvig, S. Christiansen, U. Hauss, Possible endocrine disrupting effects of  
484 parabens and their metabolites, Reprod. Toxicol. 30 (2010) 301-312.
- 485 [12] B.A.F. Hafeez, M.D.H. Maibach, An overview of parabens and allergic contact dermatitis,  
486 Skin Therapy Lett. 18 (2013) 5-6.
- 487 [13] M.G. Kirchhof, G.C. Gannes, The health controversies of parabens, Skin Therapy Lett. 18  
488 (2013) 5-7.
- 489 [14] Official Journal of the European Union, 2009. Regulation (EC) no 1223/2009 of the European  
490 Parliament and of the Council of 30 November 2009 on cosmetic products. L 342:59–209.
- 491 [15] Y. Guo, L. Wang, K. Kannan, Phthalates and parabens in personal care products from China:  
492 concentrations and human exposure, Arch. Environ. Contam. Toxicol. 66 (2014) 113-119.
- 493 [16] W. Li, Y. Shi, L. Gao, J. Liu, Y. Cai, Occurrence, fate and risk assessment of parabens and  
494 their chlorinated derivatives in an advanced wastewater treatment plant, J. Hazard. Mater. 300  
495 (2105) 29-38.
- 496 [17] W. Bae, H. Won, B. Hwang, R.A. De Toledo, J. Chung, K. Kwon, H. Shim, Characterization  
497 of refractory matters in dyeing wastewater during a full-scale Fenton process following pure-  
498 oxygen activated sludge treatment, J. Hazard. Mater. 287 (2015) 421-428.
- 499 [18] M. Panizza, G. Cerisola, Direct and mediated anodic oxidation of organic pollutants, Chem.  
500 Rev. 109 (2009) 6541-6569.
- 501 [19] F. Bonfatti, S. Ferro, F. Lavezzo, M. Malacarne, G. Lodi, A. De Battisti, Electrochemical  
502 incineration of glucose as a model organic substrate. I. Role of the electrode material, J.  
503 Electrochem. Soc. 146 (1999) 2175-2179.
- 504 [20] A. El-Ghenymy, F. Centellas, J.A. Garrido, R.M. Rodríguez, I. Sirés, P.L. Cabot, E., Brillas,  
505 Decolorization and mineralization of Orange G azo dye solutions by anodic oxidation with a

506 boron-doped diamond anode in divided and undivided tank reactors, *Electrochim. Acta* 130  
507 (2014) 568-576.

508 [21] J.R. Steter, W.R.P. Barros, M.R.V. Lanza, A.J. Motheo, Electrochemical and  
509 sonoelectrochemical processes applied to amaranth dye degradation, *Chemosphere* 117 (2014)  
510 200-207.

511 [22] E. Mousset, N. Oturan, E.D. van Hullebusch, G. Guibaud, G. Esposito, M.A. Oturan,  
512 Treatment of synthetic soil washing solutions containing phenanthrene and cyclodextrin by  
513 electro-oxidation. Influence of anode materials on toxicity removal and biodegradability  
514 enhancement, *Appl. Catal. B: Environ.* 160-161(2014) 666-675.

515 [23] M.J. Martín de Vidales, M. Millán, C. Sáez, J.F. Pérez, M.A. Rodrigo, P. Cañizares,  
516 Conductive diamond electrochemical oxidation of caffeine-intensified biologically treated  
517 urban wastewater, *Chemosphere* 136 (2015) 281-288.

518 [24] V.M. Vasconcelos, F.L. Ribeiro, F.L. Migliorini, S.A. Alves, J.R. Steter, M.R. Baldan, N.G.  
519 Ferreira, M.R.V. Lanza, Electrochemical removal of Reactive Black 5 azo dye using non-  
520 commercial boron-doped diamond film anode, *Electrochimica Acta* 178 (2015) 484-493.

521 [25] F. Sopaj, M.A. Rodrigo, N. Oturan, F.I. Podvorica, J. Pinson, M.A. Oturan, Influence of the  
522 anode materials on the electrochemical oxidation efficiency. Application to oxidative  
523 degradation of the pharmaceutical amoxicillin, *Chem. Eng. J.* 262 (2015) 286-294.

524 [26] A. Thiam, E. Brillas, F. Centellas, P.L. Cabot, I. Sirés, Electrochemical reactivity of Ponceau  
525 4R (food additive E124) in different electrolytes and batch cells, *Electrochim. Acta* 173 (2015)  
526 523-533.

527 [27] S. Aquino Neto, A.R. De Andrade, Electrooxidation of glyphosate herbicide at different DSA<sup>®</sup>  
528 compositions: pH, concentration and supporting electrolyte effect, *Electrochim. Acta* 54 (2009)  
529 2039-2045.

- 530 [28] O. Scialdone, S. Randazzo, A. Galia, G. Filardo, Electrochemical oxidation of organics at  
531 metal oxide electrode: the incineration of oxalic acid at IrO<sub>2</sub>-Ta<sub>2</sub>O<sub>5</sub> (DSA-O<sub>2</sub>) anode,  
532 Electrochim. Acta 54 (2009) 1210-1217.
- 533 [29] O. Scialdone, A. Galia, S. Randazzo, Oxidation of carboxylic acids in water at IrO<sub>2</sub>-Ta<sub>2</sub>O<sub>5</sub> and  
534 boron doped diamond anodes, Chem. Eng. J. 174 (2011) 266-274.
- 535 [30] J. Ribeiro, F.L.S. Purgato, K.B. Kokoh, J.-M. Léger, A.R. De Andrade, Application of  
536 Ti/RuO<sub>2</sub>-Ta<sub>2</sub>O<sub>5</sub> electrodes in the electrooxidation of ethanol and derivants: reactivity versus  
537 electrocatalytic efficiency, Electrochim. Acta 53 (2008) 7845-7851.
- 538 [31] A.M.Z. Ramalho, C.A. Martínez-Huitle, D.R. Da Silva, Application of electrochemical  
539 technology for removing petroleum hydrocarbons from produced water using a DSA-type  
540 anode at different flow rates, Fuel 89 (2010) 531-534.
- 541 [32] C. Salazar, I. Sirés, R. Salazar, H. Mansilla, C.A. Zaror, Treatment of cellulose bleaching  
542 effluents and their filtration permeates by anodic oxidation with H<sub>2</sub>O<sub>2</sub> production, J. Chem.  
543 Technol. Biotechnol. 90 (2015) 2017-2026.
- 544 [33] G. Ramírez, F.J. Recio, P. Herrasti, C. Ponce-de-León, I. Sirés, Effect of RVC porosity on the  
545 performance of PbO<sub>2</sub> composite coatings with titanate nanotubes for the electrochemical  
546 oxidation of azo dyes, Electrochim. Acta 204 (2016) 9-17.
- 547 [34] E. Brillas, C.A., Martinez-Huitle, Decontamination of wastewaters containing synthetic  
548 organic dyes by electrochemical methods. An updated review, Appl. Catal. B: Environ. 166-  
549 167 (2015) 603-643.
- 550 [35] L. Feng, E.D. van Hullebusch, M.A. Rodrigo, G. Esposito, M.A. Oturan, Removal of residual  
551 anti-inflammatory and analgesic pharmaceuticals from aqueous systems by electrochemical  
552 advanced oxidation processes. A review, Chem. Eng. J. 228 (2013) 944-964.
- 553 [36] F.C. Moreira, S. Garcia-Segura, R.A.R. Boaventura, E. Brillas, V.J.P. Vilar, Degradation of the  
554 antibiotic trimethoprim by electrochemical advanced oxidation processes using a carbon-PTFE

555 air-diffusion cathode and a boron-doped diamond or platinum anode, *Appl. Catal. B: Environ.*  
556 160-161 (2014) 492-505.

557 [37] A.R.F. Pipi, A.R. De Andrade, E. Brillas, I. Sirés, Total removal of alachlor from water by  
558 electrochemical processes, *Sep. Purif. Technol.* 132 (2014) 674-683.

559 [38] I. Sirés, E. Brillas, M.A. Oturan, M.A. Rodrigo, M. Panizza, Electrochemical advanced  
560 oxidation processes: today and tomorrow. A review, *Environ. Sci. Pollut. Res.* 21 (2014) 8336-  
561 8367.

562 [39] C.A. Martínez-Huitle, M.A. Rodrigo, I. Sirés, O. Scialdone, Single and coupled  
563 electrochemical processes and reactors for the abatement of organic water pollutants: A critical  
564 review, *Chem. Rev.* 115 (2015) 13362-13407.

565 [40] X. Yu, M. Zhou, G. Ren, L. Ma, A novel dual gas diffusion electrodes system for efficient  
566 hydrogen peroxide generation used in electro-Fenton, *Chem. Eng. J.* 263 (2015) 92.

567 [41] J. Vidal, C. Huiliñir, R. Salazar, Removal of organic matter contained in slaughterhouse  
568 wastewater using a combination of anaerobic digestion and solar photoelectro-Fenton  
569 processes, *Electrochim. Acta* 210 (2016) 163-170.

570 [42] G. Coria, I. Sirés, E. Brillas, J.L. Nava, Influence of the anode material on the degradation of  
571 naproxen by Fenton-based electrochemical processes, *Chem. Eng. J.* 304 (2016) 817-825.

572 [43] H. Olvera-Vargas, N. Oturan, E. Brillas, D. Buisson, G. Esposito, M.A. Oturan,  
573 Electrochemical advanced oxidation for cold incineration of the pharmaceutical ranitidine:  
574 Mineralization pathway and toxicity evolution, *Chemosphere* 117 (2014) 644-651.

575 [44] A. Thiam, I. Sirés, J.A. Garrido, R.M. Rodríguez, E. Brillas, Effect of anions on  
576 electrochemical degradation of azo dye Carmoisine (Acid Red 14) using a BDD anode and air-  
577 diffusion cathode, *Sep. Purif. Technol.* 140 (2015) 43-52.

- 578 [45] D.M. De Araújo, C. Sáez, C.A. Martínez-Huitle, P. Cañizares, M.A. Rodrigo, Influence of  
579 mediated processes on the removal of Rhodamine with conductive-diamond electrochemical  
580 oxidation, *Appl. Catal. B: Environ.* 166-167 (2015) 454-459.
- 581 [46] A. Thiam, I. Sirés, J.A. Garrido, R.M. Rodríguez, E. Brillas, Decolorization and mineralization  
582 of Allura Red AC aqueous solutions by electrochemical advanced oxidation processes, *J.*  
583 *Hazard. Mater.* 290 (2015) 34-42.
- 584 [47] J.R. Steter, D. Dionisio, M.R.V. Lanza, A.J. Motheo, Electrochemical and sonoelectrochemical  
585 processes applied to the endocrine disruptor methyl paraben, *J. Appl. Electrochem.* 44 (2014)  
586 1317-1325.
- 587 [48] J.R. Steter, R.S. Rocha, D. Dionisio, M.R.V. Lanza, A.J. Motheo, Electrochemical route of  
588 methyl paraben on a boron-doped diamond anode, *Electrochim. Acta* 117 (2014) 127-133.
- 589 [49] M.S. Lucas, J.A. Peres, Removal of emerging contaminants by Fenton and UV-driven  
590 advanced oxidation process, *Water Air Soil Poll.* 226 (2015) 273-282.
- 591 [50] T. Velegraki, E. Hapeshi, D. Fatta-Kassinos, I. Poulios, Solar-induced heterogeneous  
592 photocatalytic degradation of methyl-paraben, *Appl. Catal. B: Environ.* 178 (2015) 2-11.
- 593 [51] Y. Lin, C. Ferronato, N. Deng, F. Wu, J.-M. Chovelon, Photocatalytic degradation of  
594 methylparaben by TiO<sub>2</sub>: multivariable experimental design and mechanism, *Appl. Catal. B:*  
595 *Environ.* 88 (2009) 32-41.
- 596 [52] K.S. Tay, N.A. Rahman, M.R.B. Abas, Ozonation of parabens in aqueous solution: Kinetics  
597 and mechanism of degradation, *Chemosphere* 81 (2010) 1446-1453.
- 598 [53] E. Brillas, J.C. Calpe, J. Casado, Mineralization of 2,4-D by advanced electrochemical  
599 oxidation processes, *Water Res.* 34 (2000) 2253-2262.
- 600 [54] APWA, AWWA, WEF. Standard Methods for the Examination of Water and Wastewater. 21st  
601 Ed. Method number 4500-Cl Chlorine (residual) – G. DPD Colorimetric Method, American  
602 Public Health Association, Washington D.C., 2005, pg. 4-67 to 4-68.

- 603 [55] E.J. Ruiz, A. Hernández-Ramírez, J.M. Peralta-Hernández, C. Arias, E. Brillas, Application of  
604 solar photoelectro-Fenton technology to azo dyes mineralization: Effect of current density,  $\text{Fe}^{2+}$   
605 and dye concentration, *Chem. Eng. J.* 171 (2011) 385-392.
- 606 [56] L.P. Candeias, M.R.L. Stanford, P. Wardman, Formation of hydroxyl radicals on reaction of  
607 hypochlorous acid with ferrocyanide, a model iron(II) complex, *Free Radic. Res.* 20 (1994)  
608 241-249.
- 609 [57] N. Kishimoto, Y. Nakamura, M. Kato, H. Otsu, Effect of oxidation-reduction potential on an  
610 electrochemical Fenton-type process, *Chem. Eng. J.* 260 (2015) 590-595.
- 611 [58] A. Kapalka, G. Fóti, C. Comninellis, Kinetic modelling of the electrochemical mineralization  
612 of organic pollutants for wastewater treatment, *J. Appl. Electrochem.* 38 (2008) 7-16.
- 613 [59] M.E.H. Bergmann, J. Rollin, T. Iourtchouk, The occurrence of perchlorate during drinking  
614 water electrolysis using BDD anodes, *Electrochim. Acta* 54 (2009) 2102-2107.
- 615 [60] O. Azizi, D. Hubler, G. Schrader, J. Farrell, B.P. Chaplin, Mechanism of perchlorate formation  
616 on boron-doped diamond film anodes, *Environ. Sci. Technol.* 45 (2011) 10582-10590.
- 617 [61] Z. Lin, W. Yao, Y. Wang, G. Yu, S. Deng, J. Huang, B. Wang, Perchlorate formation during  
618 the electro-peroxone treatment of chloride-containing water: Effects of operational parameters  
619 and control strategies, *Water Res.* 88 (2016) 691-702.
- 620 [62] H. Wang, B. Bakheet, S. Yuan, X. Li, G. Yu, S. Murayama, Y. Wang, Kinetics and energy  
621 efficiency for the degradation of 1,4-dioxane by electro-peroxone process, *J. Hazard. Mater.*  
622 294 (2015) 90-98.
- 623 [63] P. Frangos, H.J. Wang, W.H. Shen, G. Yu, S. Deng, J. Huang, B. Wang, Y.J. Wang, A novel  
624 photoelectro-peroxone process for the degradation and mineralization of substituted benzenes  
625 in water, *Chem. Eng. J.* 286 (2016) 239-248.

626 [64] W. Shen, Y. Wang, J. Zhan, B. Wang, J. Huang, S. Deng, G. Yu, Kinetics and operational  
627 parameters for 1,4-dioxane degradation by the photoelectro-peroxone process, Chem. Eng. J.  
628 [doi:org/10.1016/j.cej.2016.10.111](https://doi.org/10.1016/j.cej.2016.10.111).

629

630 **Figure captions**

631 **Figure 1.** Variation of the concentration of: (●) active chlorine and (○) accumulated H<sub>2</sub>O<sub>2</sub> with  
632 electrolysis time for 100 mL of a 0.025 M Na<sub>2</sub>SO<sub>4</sub> + 0.035 M NaCl solution with 0.50 mM Fe<sup>2+</sup> at  
633 pH 3.0 under EF conditions with a BDD/air-diffusion cell at 66.7 mA cm<sup>-2</sup> and 35 °C.

634 **Figure 2.** TOC removal with electrolysis time for the treatment of 100 mL of 158 mg L<sup>-1</sup>  
635 methylparaben in 0.025 M Na<sub>2</sub>SO<sub>4</sub> + 0.035 M NaCl at pH 3.0 by different EAOPs using cells of 3  
636 cm<sup>2</sup> electrode area containing an air-diffusion cathode and operating at 66.7 mA cm<sup>-2</sup> and 35 °C. (a)  
637 (●) EO-H<sub>2</sub>O<sub>2</sub>, (■) EF with 0.50 mM Fe<sup>2+</sup> and (▲) PEF with 0.50 mM Fe<sup>2+</sup> using a BDD anode.  
638 (b) EO-H<sub>2</sub>O<sub>2</sub> with a (◆) Pt, (◇) IrO<sub>2</sub>-based and (▼) RuO<sub>2</sub>-based anode. PEF with a (○) Pt, (□)  
639 IrO<sub>2</sub>-based and (△) RuO<sub>2</sub>-based anode.

640 **Figure 3.** TOC decay vs. electrolysis time for the same methylparaben solutions of Fig. 2, but using  
641 0.050 M Na<sub>2</sub>SO<sub>4</sub> as background electrolyte. (a) (●) EO-H<sub>2</sub>O<sub>2</sub>, (■) EF and (▲) PEF with a BDD  
642 anode. (b) EO-H<sub>2</sub>O<sub>2</sub> with a (◆) Pt, (◇) IrO<sub>2</sub>-based and (▼) RuO<sub>2</sub>-based anode. PEF with a (○) Pt,  
643 (□) IrO<sub>2</sub>-based and (△) RuO<sub>2</sub>-based anode.

644 **Figure 4.** TOC abatement with electrolysis time for the same methylparaben solutions of Fig. 2, but  
645 using 0.070 M NaCl. (a) (●) EO-H<sub>2</sub>O<sub>2</sub>, (■) EF and (▲) PEF with a BDD anode.

646 **Figure 5.** Change of mineralization current efficiency with electrolysis time for the trials of Fig. 2.  
647 (a) (●) EO-H<sub>2</sub>O<sub>2</sub>, (■) EF and (▲) PEF with a BDD anode. (b) EO-H<sub>2</sub>O<sub>2</sub> with a (◆) Pt, (◇) IrO<sub>2</sub>-  
648 based and (▼) RuO<sub>2</sub>-based anode. PEF with a (○) Pt, (□) IrO<sub>2</sub>-based and (△) RuO<sub>2</sub>-based anode.

649 **Figure 6.** Variation of specific energy consumption per unit TOC mass with electrolysis time for  
650 the assays of Fig. 2. (a) (●) EO-H<sub>2</sub>O<sub>2</sub>, (■) EF and (▲) PEF with a BDD anode. (b) EO-H<sub>2</sub>O<sub>2</sub> with  
651 a (◆) Pt and (▼) RuO<sub>2</sub>-based anode. PEF with a (○) Pt, (□) IrO<sub>2</sub>-based and (△) RuO<sub>2</sub>-based  
652 anode.

653 **Figure 7.** Decay of methylparaben concentration with electrolysis time for 100 mL of 158 mg L<sup>-1</sup> of  
654 compound in 0.025 M Na<sub>2</sub>SO<sub>4</sub> + 0.035 M NaCl at pH 3.0 using a BDD/air-diffusion cell at 66.7  
655 mA cm<sup>-2</sup> and 35 °C. (a) (●) EO-H<sub>2</sub>O<sub>2</sub> and (■) EF. (b) PEF. The kinetic analysis for a pseudo-first-  
656 order reaction for methylparaben is presented in the inset panel of (a).

657 **Figure 8.** Time course of methylparaben concentration for 100 mL of 158 mg L<sup>-1</sup> of compound in  
658 0.050 M Na<sub>2</sub>SO<sub>4</sub> at pH 3.0 using a BDD/air-diffusion cell at 66.7 mA cm<sup>-2</sup> and 35 °C. (a) EO-H<sub>2</sub>O<sub>2</sub>.  
659 (b) (■) EF and (▲) PEF. The inset panel of (a) shows the kinetic analysis assuming a pseudo-first-  
660 order reaction for methylparaben.

661 **Figure 9.** Reaction sequence proposed from GC-MS determination for methylparaben  
662 mineralization in 0.025 M Na<sub>2</sub>SO<sub>4</sub> + 0.035 M NaCl by EAOPs with a BDD/air-diffusion cell.  
663 Hydroxyl radicals, •OH, account for either adsorbed (M(•OH)) or homogeneous radicals.

664 **Figure 10.** Route proposed from GC-MS determination for methylparaben mineralization in 0.050  
665 mM Na<sub>2</sub>SO<sub>4</sub> by EAOPs with a BDD/air-diffusion cell. Hydroxyl radicals, •OH, account for either  
666 adsorbed (M(•OH)) or homogeneous radicals.

667 **Figure 11.** Time course of oxalic acid concentration detected during the degradation of 100 mL of  
668 158 mg L<sup>-1</sup> methylparaben at pH 3.0 by EAOPs at 66.7 mA cm<sup>-2</sup> and 35 °C. (a) BDD/air-diffusion  
669 cell using (●) EO-H<sub>2</sub>O<sub>2</sub>, (■) EF and (▲) PEF with 0.050 M Na<sub>2</sub>SO<sub>4</sub>, and (◆) PEF with 0.025 M  
670 Na<sub>2</sub>SO<sub>4</sub> + 0.035 M NaCl. (b) PEF with a (○) Pt/air-diffusion, (□) IrO<sub>2</sub>-based/air-diffusion and (△)  
671 RuO<sub>2</sub>-based/air-diffusion cell with 0.050 M Na<sub>2</sub>SO<sub>4</sub>.